Evaluation of Water Permittivity Models From Ground-Based Observations of Cold Clouds at Frequencies Between 23 and 170 GHz

Maria P. Cadeddu and David D. Turner

***Abstract*—Accurate retrievals of liquid water path (LWP) from passive microwave radiometers rely on the use of radiative transfer models to describe the absorption of radiation by various atmospheric components. When clouds are present, atmospheric absorption is affected by the dielectric properties of liquid water. In this paper, we use measurements from four microwave radiometers to assess four models of the complex permittivity of water. The observations are collected at five frequencies between 23.8 and 170 GHz. The purpose of the study is to compare measurements of microwave absorption with model computations in supercooled liquid clouds that have temperatures between 0 °C and −30 °C. Models of liquid water permittivity in this temperature range suffer from a lack of laboratory measurements and are generally derived from the extrapolation of available data. An additional rationale for this work is to examine to what degree the use of different dielectric models affects the retrieval of LWP in supercooled liquid clouds. Inaccuracies in modeling the water permittivity at low temperatures are likely one of the largest sources of retrieval uncertainty in supercooled clouds, uncertainty that could offset the advantages offered by the enhanced sensitivity of channels at frequencies at and above 90 GHz relative to lower frequencies.**

***Index Terms*—Cloud liquid absorption models, liquid water path retrievals, microwave radiometry, water permittivity.**

I. Introduction

SEVERAL physical models describing the dielectric properties of water in an electromagnetic field of microwave radiation have been published (see among others [1]–[4]). Passive microwave remote sensing of clouds depends critically on the accurate modeling of such dielectric properties. The retrieval of cloud liquid water is an important aspect of microwave remote sensing because the earth radiative balance is strongly affected by cloud cover (e.g., [5]). Ground-based microwave radiometry has traditionally relied on the use of frequencies between 20 and 60 GHz for the retrieval of precipitable water vapor (PWV) and liquid water path (LWP) (e.g., [6], [7]). However, because of the propensity of clouds with small LWP amounts and the importance of these clouds [5], [7], the community has recently started using higher frequencies, in the 90–200 GHz region. These frequencies have higher sensitivity to small amounts of cloud liquid water and thereby can improve the retrieval of liquid water by reducing the random uncertainties in the current LWP retrievals [8]. The spectral region above 90 GHz, however, is also where models of water permittivity tend to have larger differences. Previous studies have demonstrated that dielectric models exhibit discrepancies even at 20–30 GHz at temperatures below −10 °C and have estimated the effect of such differences on LWP retrievals [9], [10]. Similarly Lipton *et al.* [11] showed that the use of different absorption models has a non-negligible effect on LWP retrievals. Other studies have used measurements from microwave radiometers to evaluate models of dielectric permittivity (e.g., [4], [12]), and some have proposed new parameterizations by deriving new fits to existing laboratory data sets [4], [13].

Although ground-based radiometers have been recognized to be an important tool for improving radiative transfer models, validation efforts have focused mainly on the study of water vapor (lines and continuum) [14]–[16] and oxygen absorption [17]. Part of the problem in assessing the performance of water permittivity models is the difficulty in obtaining independent measurements of LWP and the need for observations in supercooled liquid clouds conditions.

In this paper, we combine observations from four microwave radiometers spanning a frequency range between 23.8 and 170 GHz. Brightness temperatures measured by the radiometers are used to compute mass absorption coefficients due to liquid water that are then compared to calculations performed with four complex permittivity models [3], [18]–[20] hereafter referred to as Liebe-91, Liebe-93, Stogryn-95, and Ellison-06 models, respectively. Data from several additional instruments are used in the selection and preparation of the data set. Data from a cloud radar were used to select single-layer clouds, and a ceilometer was used to identify the location of the cloud base. Radiosondes were used to provide vertical profiles of

Manuscript received October 4, 2010; revised February 4, 2011; accepted February 20, 2011. Date of publication April 29, 2011; date of current version July 22, 2011. This work was supported by the Office of Advanced Scientific Computing Research, Office of Science, U.S. Department of Energy, under Contract DE-AC02-06CH11357 and by the Grant DE-FG02-06ER64167 from DOE as part of the ARM program.

M. P. Cadeddu is with Argonne National Laboratory, Argonne, IL 60439 USA (e-mail: mcadeddu@anl.gov).

D. D. Turner was with University of Wisconsin-Madison, Madison, WI 53706 USA. He is currently with NOAA/National Severe Storms Laboratory, Norman, OK 73072 USA (e-mail: dave.turner@noaa.gov).

Color versions of one or more of the figures in this paper are available online at http://ieeexplore.ieee.org.

Digital Object Identifier 10.1109/TGRS.2011.2121074

temperature and humidity as well as the average temperature of the cloud layer. An Atmospheric Emitted Radiance Interferometer (AERI) and a Micropulse Lidar were used to obtain independent retrievals of LWP to use as input to the simulations. LWP retrievals from AERI are crucial for this analysis; however, they also limit the sampling to cases of relatively low LWP clouds, as discussed later.

In Section II the design and calibration of the radiometers are briefly described and clear-sky measurements are compared with model simulations to characterize the total level of uncertainty we can expect in our comparison. In Section III the permittivity models used in this study are briefly presented and compared with each other. A comparison between the measurements and model simulations during cloudy conditions is shown in Section IV, where the results and implications for the LWP retrieval are discussed. Section V concludes the study with a brief discussion of results.

II. Instruments and Measurement

A. Radiometers and Their Calibration

The four radiometers used in this study are part of the U.S. Department of Energy (DOE) Atmospheric Radiation Measurement (ARM) Program Climate Research Facilities [21]. Two of the radiometers are located at the Southern Great Plains (SGP, 36.6° N, −97.5° E) site in Oklahoma and include a two-channel microwave radiometer (MWR) [7] operating at 23.8 and 31.4 GHz and a microwave radiometer high-frequency (MWRHF) [16] operating at 90 and 150 GHz. The two remaining radiometers are located at the North Slope of Alaska (NSA, 71.3° N, −156.8° E) site. Of these one is an MWR similar to that in Oklahoma, and the second is the G-band vapor radiometer profiler (GVRP) [22], a millimeter-wave radiometer with 15 channels between 170 and 183.31 GHz.

The radiometers are calibrated with different methodologies and algorithms. The two MWRs are calibrated by using tip curves as explained in [23]. Calibration uncertainty in the observed sky brightness temperature for these instruments is estimated to be of the order of 0.3 K. The MWRHF is also calibrated by using tip curves. The algorithm, which is similar in many respects to that in [23], processes tip curves in real time to track the drift of the effective noise diode temperature (T_{nd}), and continuously updates the calibration of the instrument by using a black body target as the second reference. The two channels (90 and 150 GHz) are independently calibrated by computing the median value of the last 50 instantaneous T_{nd} values derived from the tip curves that passed a threshold criterion. During observations, a slight drift occurred in the noise diode of the 150 GHz receiver. The calibration algorithm was able to detect and account for this drift. Since the instrument (including the feed horn and antenna) is thermally stabilized to 30 mK, there was no need to account for thermal fluctuations due to exposed receiver components. It is estimated that with this calibration algorithm, a 1 K error in the calibration of the noise diode will result in a 0.3 K error in the calibrated brightness temperature of the 90 GHz channel and a 0.2 K error in the brightness temperature of the 150 GHz channel. Differences between T_{nd} estimated with liquid nitrogen (LN_2) calibrations and T_{nd} estimated with tip curves were of the order of 4 K for the 90 GHz channel and 6 K for the 150 GHz channel (before the drift), placing the brightness temperature calibration uncertainty at about 1 K for both channels. From repeated LN_2 calibrations it was estimated that 1 K can also be considered a low estimate of uncertainty for the LN_2 calibrations of these channels. The GVRP is routinely calibrated with liquid nitrogen. Of the 15 calibrated frequencies in this study, we used only the 170 GHz channel. LN_2 calibration of this transparent channel was double-checked with tip curves, as the clear sky atmospheric opacity at the NSA site was small enough at this frequency to allow successful tip curves to be collected. A linear correction was applied to the effective noise diode temperature to account for residual temperature dependencies of the receiver components. A reasonable estimate of calibration uncertainty for this instrument can be placed at 1 K.

B. Clear-Sky Measurements

An important and necessary part of the study is the examination of measurements collected during clear-sky conditions and their comparison with simulations. This exercise characterizes the uncertainties that derive from calibration, from modeling of the water vapor continuum, and from variability in the calibration of the radiosonde's humidity sensor. Clear-sky data were collected during the same months and in the same locations as the cloudy data: during the 2008–2009 winter at the SGP and during March 2007 at the NSA. Vaisala RS92 radiosondes were launched four times a day at the SGP site and twice a day at the NSA site during these periods. To eliminate possible effects due to a diurnal dry bias [24], the radiosondes relative humidity was scaled with the PWV derived from the MWR at the SGP and from the G-band vapor radiometer (GVR) [25], [26] at the NSA.

The gaseous absorption model used in this study is MonoRTM [27]. The water vapor continuum model used for the simulations is the one proposed in [16]. In this formulation, the self and foreign components of the water vapor continuum were scaled to minimize the residuals between the model and measurements collected by two ground-based microwave radiometers similar to the MWRHF. Fig. 1 shows the clear-sky differences between modeled and measured brightness temperatures for the 31.4, 90, 150, and 170 GHz channels. Table I shows corresponding values of biases and standard deviations for all instruments and all channels. The mean of the clear sky residuals is within the stated calibration uncertainty of less than 1 K for all channels. The standard deviation of the high-frequency channels (MWRHF and GVRP) is between 1 and 2 K. The magnitude of the standard deviation reflects the uncertainty due to sampling inconsistencies (e.g., the drift of the radiosondes away from the radiometer locations), atmospheric variability, and random instrument noise. The clear-sky comparison indicates that, at least during the time examined, there was no appreciable bias between the model and the clear-sky measurements for the high-frequency channels. Only the MWR located at the NSA displays a clear-sky bias of the 23.8 GHz channel that is slightly above the expected 0.3 K calibration uncertainty. Although some results for this channel

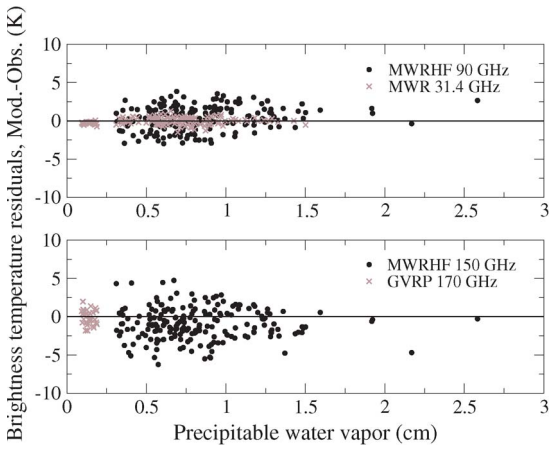

Fig. 1. Downwelling brightness temperature residuals (modeled—measurements) for clear-sky cases. Top panel: 90 GHz channel at the SGP (black circles); 31.4 GHz channel at the SGP and NSA (brown crosses). Bottom panel: 150 GHz channel at the SGP (black circles); 170 GHz channel at the NSA (brown crosses). Corresponding numerical values are displayed in Table I.

TABLE I
CLEAR-SKY DIFFERENCES BETWEEN MODELED AND MEASURED DOWNWELLING BRIGHTNESS TEMPERATURES FOR THE MWR, MWRHF, AND GVRP. IN THE LAST ROW ARE THE MINIMUM, MAXIMUM, AND AVERAGE VALUES OF THE PWV (cm) AT THE SITE DURING THE TIME OF THE OBSERVATIONS

Frequency (GHz)	SGP ΔTb (K)		NSA ΔTb (K)	
	MWR N=121	MWRHF N=192	MWR N=36	GVRP N=36
23.8	0.039±0.283		–0.47±0.12	
31.4	0.005±0.467		–0.28±0.15	
90.		0.32±1.60		
150.		0.96±2.06		
170.				–0.12±0.91
PWV	0.31, 2.58, 0.83		0.09, 0.19, 0.14	

are discussed later, the 23.8 GHz frequency has a very limited sensitivity to liquid water; and, especially at the NSA, the contribution to the brightness temperatures is almost entirely due to water vapor and oxygen.

III. MODELS OF COMPLEX PERMITTIVITY OF WATER

A. Description of the Models

The water permittivity models examined in this study provide a fit for the complex dielectric constant of pure water. All models are derived from experimental laboratory data collected in a range of temperatures spanning from 0 °C to 20 °C (or sometimes 40 °C). It is desirable to gain some knowledge of how the models compare with measurements in cases of supercooled clouds, when the cloud temperature is well below the range of the laboratory settings.

The response of a dielectric medium exposed to a field of microwave radiation is traditionally modeled through a complex-Debye relaxation function or through one of its variants such as the Cole–Cole function. These functions depend on radiation frequency, temperature, and a relaxation time constant. The relaxation function consists of a high-frequency term usually indicated with $\varepsilon_\infty(T)$ and a low-frequency (or static) term $\varepsilon_0(T)$. The function is of the type

$$\varepsilon(\nu,T)=\varepsilon_\infty+\frac{\varepsilon_0-\varepsilon_\infty}{1-i\nu 2\pi\tau} \tag{1}$$

where ν is the frequency and $\tau(T)$ is the relaxation time. The first model analyzed here is the one proposed in [3] (Liebe-91). In this model the singleDebye function shown in (1) was modified with the addition of a third term

$$\varepsilon(\nu,T)=\varepsilon_\infty+\frac{\varepsilon_0-\varepsilon_1}{1-i2\pi\tau_1\nu_1}+\frac{\varepsilon_1-\varepsilon_\infty}{1-i2\pi\tau_2\nu_2}. \tag{2}$$

The temperature dependence of the function comes from fitting the terms ε_∞, ε_0, ε_1, τ_1 and τ_2 as a function of temperature. This "double-Debye" fit was deemed necessary to accommodate experimental data at frequencies below 1 THz. Two possible fits were proposed for the first relaxation frequency $(1/2\pi\tau_1)$: a quadratic fit and an exponential fit. In this paper, the quadratic fit is analyzed. Although the Liebe-91 fit showed a reasonable behavior at lower frequencies and temperatures above 0 °C it displayed unrealistic behavior above 90 GHz and at cold temperatures. In a following work, Liebe [18] (Liebe-93) offered a modification of the model to improve the behavior at frequencies above 90 GHz and at colder temperatures below -10 °C. The Liebe-93 model kept the double-Debye fit but eliminated any temperature dependence from the high-frequency term ε_∞. The third and fourth models examined are also double-Debye fits. In the Ellison-06 model [20] the temperature dependence of the various terms is modeled with exponential rather than polynomial functions. The fourth model is from [19] (Stogryn-95).

B. Model Comparison

Fig. 2 shows sky brightness temperature differences produced by the four models (expressed as Liebe-91 minus the other models) as a function of LWP for three average cloud temperatures: one cold case ($T_{\rm avg}=-19$ °C) one intermediate case ($T_{\rm avg}=-9$ °C) and one warm case ($T_{\rm avg}=+10$ °C). At 90 GHz (left column), the four models produce brightness temperatures that are within a few degrees of each other except in the case of thick clouds with large LWP values. At 90 GHz, the Stogryn-95 model generally produces lower brightness temperatures, especially at cold temperatures. At 150 GHz the Ellison-06 model produces results similar to those of Liebe-91. On the other hand, the Liebe-93 and Stogryn-95 models produce slightly lower brightness temperatures. Differences between the models are more pronounced in cold clouds, and they increase with LWP. They are generally less than 2 K in warmer clouds when temperatures are above freezing. The differences between the four liquid water models at 170 GHz are similar to the results at 150 GHz, and thus are not shown.

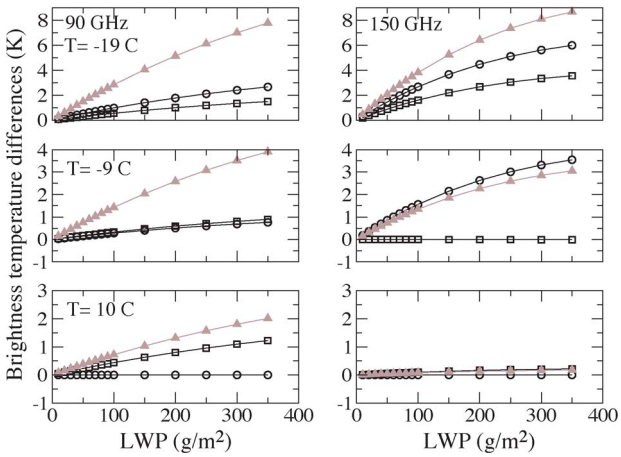

Fig. 2. Model differences at three representative cloud temperatures (−19 °C, −9 °C, and +10 °C from top to bottom) for the two MWRHF frequencies: 90 GHz (left column) and 150 GHz (right column). The symbols represent: Liebe-91 minus Liebe-93 (circles), Liebe-91 minus Ellison-06 (squares), and Liebe-91 minus Stogryn-95 (brown triangles).

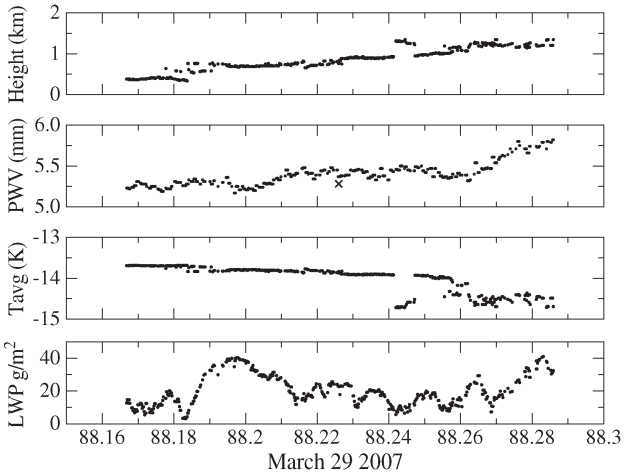

Fig. 3. Sample of data used in the NSA comparison. From the top: Cloud base height from Vaisala ceilometer; PWV retrieved from the GVR (black dots) and derived from the radiosonde (cross); estimated cloud average temperature; AERI-retrieved LWP.

For thin clouds (i.e., with LWP of less than 100 g/m^2) the differences between the models are relatively small, typically in the order of 2–3 K in all temperature regimes. The simulation in Fig. 2 illustrates the primary difficulty encountered in this study. To have an independent measure of LWP from AERI we must limit our comparison to single-layer clouds with LWP below 55 g/m^2 [28], [29]. Differences between the models in this LWP range are small, of the order of 2 K at most. Thus, if the Liebe-91 model produces brightness temperatures that are too warm at 150 and 170 GHz relative to the observations, we would expect to detect slightly larger positive residuals (model—measurements) only in cases of extremely cold clouds. If, on the other hand, the Liebe-93 and Stogryn-95 models produce temperatures that are too cold, we can expect slightly larger negative residuals for these models in very cold clouds as well. From the 90 GHz measurements it will not be possible to detect which model is closer to the observations due to the lack of spread among the sensitivities of the different models for these low LWP conditions used in our study, but we can have an idea of how well all models compare with the observations.

IV. Comparison With Measurements

A. Data Set Description

Data used in this study were collected at two of the ARM Climate Research Facility sites. Several periods of single-layer supercooled liquid clouds were examined at the SGP during a four-month period from November 2008 to February 2009. At the NSA two periods were identified during March 2007. Near-coincident data from a Vaisala ceilometer, radiosondes, and AERI were analyzed in addition to the measurements from the microwave radiometers. Data were collected in temporal proximity (±1 hour) of radiosondes launches, during which time the atmospheric temperature profile could be assumed to be stable.

Fig. 3 provides an example of the data used in the analysis. This period includes 483 points collected at the NSA in March 2007. The top panel shows the temporal evolution of the cloud base height derived from the Vaisala ceilometer. The uncertainty associated with this measurement is roughly 100 m. Because of the low sensitivity of microwave radiometers to the location of the clouds, this measurement will not constitute a large source of uncertainty in the following analysis. The second panel [Fig. 3(b)] shows the corresponding PWV derived from the microwave radiometer (the GVR in this specific case; the MWR for cases at the SGP). The cross indicates the PWV measured by the radiosonde. Because the same radiosonde launch is used to perform radiative transfer computation throughout the whole time period, the radiosonde relative humidity is scaled at each sample time with the PWV retrieved from the microwave radiometer. The temperature profile measured by the radiosondes is used to estimate the average temperature of the cloud layer [Fig. 3(c)]. From the uncertainty in the measurement of the cloud base height we can safely assume an error of $\sim \pm 5$ K in the estimation of the average cloud temperature. Fig. 3(d) shows the LWP retrieved from AERI.

Independent retrievals of LWP are necessary to compare the observed sky brightness temperatures from the various microwave radiometers with simulations in cloudy conditions. Unfortunately, microwave radiometers are the only instruments that can provide reliable measurements of LWP under a wide range of cloud conditions. The AERI measures sky infrared radiances between 400 and 3000 cm^{-1} with spectral resolution of 1 cm^{-1}. The downwelling infrared radiance is sensitive to liquid water clouds; however, the infrared spectrum becomes opaque and loses sensitivity when the LWP is greater than approximately 60 g/m^2[29]. The instrument calibrates with one hot target (∼60 °C) and one ambient target, and thus its absolute accuracy is better than 1% of the ambient radiance [30].

The mixed-phase cloud property retrieval algorithm (MIXCRA) is used to retrieve LWP from the AERI. The algorithm retrieves cloud liquid and ice water path (among other parameters) from infrared radiances and lidar cloud

boundary observations. MIXCRA can provide accurate LWP retrievals when the LWP is less than 60 g/m^2 [29]. In addition, MIXCRA can distinguish between liquid and ice phase in situations of low water vapor (PWV < 1 cm). Dual-phase retrievals were used in this study when the average cloud temperature was below -15 °C. If the PWV is too high and the water phase cannot be separated the resulting retrievals will overestimate the amount of liquid (if ice is present in the cloud); however, the lidar data set was visually inspected, and cases that appeared to contain ice were eliminated. LWP retrieval errors increase with the LWP; for this data set, the 2-sigma MIXCRA LWP uncertainty ranges between 0.5 and 4 g/m^2 as the LWP ranges from 5 to 55 g/m^2 (Fig. 3 in [29]). Uncertainty in the MIXCRA retrieval, especially if a very small amount of undetected ice is in the cloud, is one of the largest sources of uncertainty in this analysis and may account for some of the scatter observed in the comparison.

For all our cases, MonoRTM calculations were made using the four different liquid water absorption models, where the LWP was determined from the MIXCRA retrievals. In the simulations the liquid water of the cloud layer was uniformly distributed between the estimated cloud boundaries. The error associated with this assumption is virtually negligible in our study because microwave radiometers are largely insensitive to the vertical distribution of liquid, especially when the LWP is small [31], and the vertical extent of our clouds is fairly small (less than 750 m in all cases, with a mean of 350 m).

Several sources of uncertainty impact the subsequent analysis. Besides the noise caused by natural atmospheric variability occurring during and near the radiosondes launches, uncertainties in the location of the cloud affect the estimation of the average cloud temperature, although this uncertainty is considered to be very small. Uncertainties in the retrieved PWV and, particularly, LWP affect the computation of the simulated brightness temperatures, for example an error of 5 g/m^2 in the retrieved LWP results in an error of $\sim$1 K and 1.2 K in the simulated brightness temperatures at 90 and 150 GHz, respectively. The compounded effect of all these sources of uncertainty results in a spread of the computed brightness temperatures. In the low LWP regime analyzed here, the spread between the models is in most cases within the uncertainty level of the measurements. However, the data set still provides us with useful insights regarding the general behavior of the models, especially at higher frequencies and at very cold temperatures. Based on the standard deviation of the clear-sky cases and on the sensitivity of each channel to changes in LWP, a lower LWP threshold of 10 g/m^2 was used to eliminate cases that may fall within the clear-sky variability of the measurements. The final data set includes a total of 1331 cases at the SGP and 588 cases at the NSA.

B. Mass Absorption Coefficient Comparison

Before we proceed with the brightness temperature comparison, it is useful to compare the modeled and estimated (from the observations) mass absorption coefficients. The mass absorption coefficient is independent of the LWP, and it is directly related to the dielectric constant of liquid water. In the Rayleigh approximation the cloud absorption $\alpha_{\rm L}$ at frequency ν for a cloud of liquid density $\rho_{\rm L}$ is computed as

$$\alpha_L \sim 6\pi\nu\rho_L \mathrm{Im}\left(\frac{\varepsilon-1}{\varepsilon+2}\right) \sim \frac{\varepsilon''}{(\varepsilon'+2)^2+\varepsilon''^2} \tag{3}$$

where ε is the complex dielectric constant of water defined in (1) and ε' and ε'' are its real and imaginary parts, respectively. A path-averaged mass absorption coefficient can also be defined as

$$\overline{\alpha_L} = \frac{\int_0^\infty \alpha_L(z,\nu)\rho_L(z)\,dz}{\int_0^\infty \rho_L(z)\,dz}. \tag{4}$$

This averaged mass absorption coefficient can be expressed as $\overline{\alpha}_{\rm L} = \tau_{\rm L}/{\rm L}$, where L is the LWP and $\tau_{\rm L}$ is the component of the opacity due to liquid water. To compare the modeled and measured mass absorption coefficient, it is necessary to estimate $\overline{\alpha}_{\rm L}$ from the measurements. To do so, we first estimate the total opacity from the measurements

$$\tau = \ln\left(\frac{T_{\rm mr}-T_{\rm c}}{T_{\rm mr}-T_{\rm b}}\right) \tag{5}$$

where $T_{\rm mr}$ is the calculated mean radiating temperature at each frequency [32], $T_{\rm c}$ the cosmic background, and $T_{\rm b}$ the corresponding measured brightness temperature. We then compute the dry (oxygen and nitrogen) and water vapor components of the opacity with a radiative transfer model and estimate the component due to the liquid as $\tau_{\rm L} = \tau - \tau_{\rm d} - \tau_{\rm wv}$. In this way the mass absorption coefficient due to the liquid can be estimated from the measurements and compared with that directly calculated from the model. The non-liquid components ($\tau_{\rm d}$ and $\tau_{\rm wv}$) were calculated by integrating the absorption coefficients due to vapor, oxygen, and nitrogen over the whole atmosphere. Obviously errors in the calculations of $\tau_{\rm d}$ and $\tau_{\rm wv}$ have an impact on the estimated $\tau_{\rm L}$. The clear-sky brightness temperature comparison does not display a dependence of the residuals on the mean atmospheric temperature and the range of PWV in the data set is limited; therefore, we do not expect temperature-dependent systematic errors in the water vapor and dry components of the opacity. Estimated liquid absorption coefficients were binned in sliding 10-degree temperature intervals. Fig. 4 shows the temperature dependence of the model predicted mass absorption coefficient for each model, along with the estimated $\overline{\alpha}_{\rm L}$ for all frequencies. Numerical values of the mean and standard deviation for each bin are shown in Table II. All models have similar temperature dependence for temperatures warmer than approximately -20 °C for the 23.8 and 31.4 GHz (Fig. 4, top two panels), and all models seem to agree with the measurements within the uncertainties of the observations at these two frequencies. However, at 90 and 150 GHz, the differences among the models are more noticeable, especially for temperatures below -15 °C, with the largest differences being between the Liebe-91 and Stogryn-95 models that predict opposite behavior of the absorption coefficients at these low temperatures.

In Fig. 4 the permittivity models were extrapolated to temperatures well below the range where laboratory measurements are

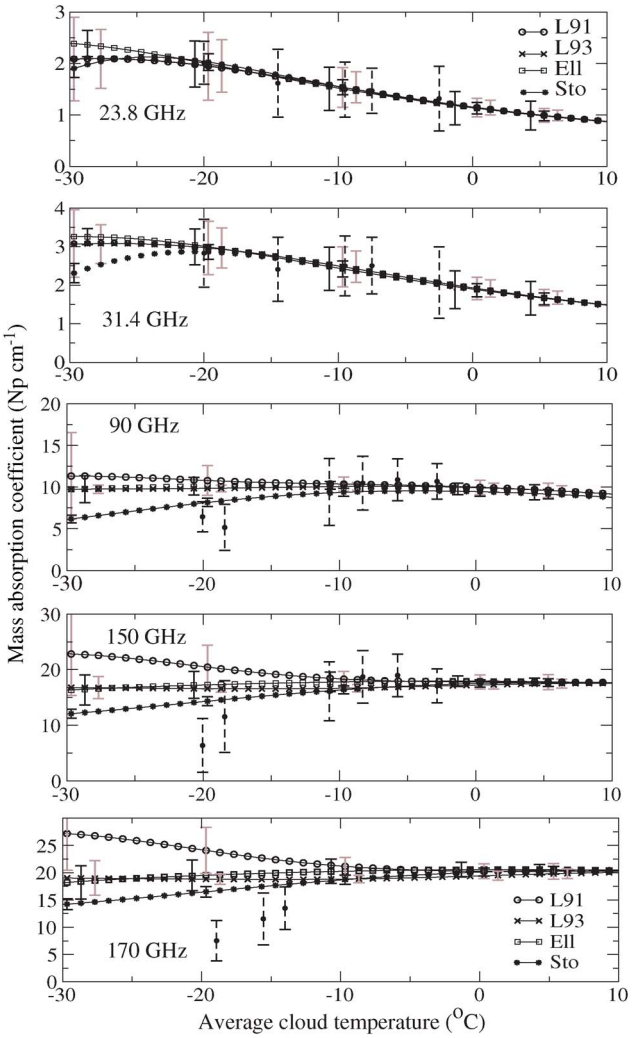

Fig. 4. Estimated and calculated mass absorption coefficients for the 5 frequencies used in this study: 23.8, 31.4, 90.0, 150.0, and 170.0 GHz (top to bottom, respectively). Points with dashed error bars (± 1 standard deviation) are estimated from brightness temperature measurements. The models are Liebe-91 (circles), Liebe-93 (crosses), Ellison-06 (squares), and Stogryn-95 (stars). Solid error bars correspond to the uncertainty associated with a 5% perturbation of each model parameter. Corresponding numerical values for the mass absorption coefficients estimated from the observations, including the number of points per observation bin, are provided in Table II.

available. It is therefore important to estimate how uncertainties in the model parameters are propagated in the process of extrapolation. For this reason a 5% perturbation was applied to the model parameters and the resulting uncertainty in the absorption coefficient was computed as:

$$\sigma^2_{\mathrm{mod}} = \sum_{i=1,N} \sigma_i^2 \left(\frac{\partial \alpha_L}{\partial p_i} \right)^2 \tag{6}$$

where the standard deviation on each parameter was assumed to be $\sigma_{\mathrm{i}} = 5\%$ and N is the number of fitting parameters. The results from this exercise are shown in Fig. 4 as vertical bars centered on the models at selected temperatures. The Liebe-91 model shows the greatest sensitivity to a small perturbation of the parameters followed by the Ellison model. In both models the largest uncertainties are related to the temperature dependence of the first relaxation frequency $1/2\pi\tau_1$. In all models, however, larger deviations would be necessary to make the experimental data a better fit.

The observations seem to support the Stogryn-95 model at both frequencies, with the absorption coefficient decreasing slightly at very cold temperatures. All models agree with the measurements fairly well when the temperature is above roughly -15 °C at 90 and 150 GHz. The bottom panel of Fig. 4 shows the estimated mass absorption coefficient at 170 GHz. In this case again the observations seem to support the general behavior of the Stogryn-95 model, although the temperature dependence is more pronounced in the data. Again the Liebe-91 model (with the quadratic fit) has the largest discrepancy with the measurements. The results are consistent with the concern (expressed in [18]) that the Liebe-91 fit had a poor behavior at low temperature for frequencies above 90 GHz. The temperature dependence of the Liebe-93 and Ellison-06 models appears to be weaker than what is suggested by the measurements.

The frequency dependence of the absorption coefficient calculations for the four models together with that estimated from the measurements at four temperatures (-20 °C, -14 °C, -8 °C, and -3 °C) is shown in Fig. 5. At the coldest temperature [Fig. 5(a)] the discrepancy between all models and the measurements increases with frequency, suggesting that the absorption in all models at this temperature (-20 °C) is too strong. For the other three temperatures [Fig. 5(b)–(d)] the measurements are in much better agreement with the models.

The MIXCRA retrievals used in this analysis assumed the refractive index of liquid water as determined by Downing and Williams [33]. This formulation does not have any temperature dependence to the liquid water refractive indices in the thermal infrared; however, some recent laboratory studies have suggested that there is temperature dependence that impacts the infrared absorption for supercooled liquid water drops [34], [35]. However, when we utilize the temperature-dependent refractive indices of [34] in the MIXCRA retrievals, the quality of the retrievals actually decreases; in other words, the fit to the infrared spectrum is slightly worse than when the original refractive indices of [33] are used. Furthermore, if we use the Zasetsky *et al.* temperature-dependent refractive indices in MIXCRA, the retrieved LWP values are approximately 10 g/m^2 larger than when the Downing and Williams indices are used; however, this increase results in a significantly larger liquid water opacity that translates into a much larger average mass absorption coefficient that is not at all consistent with published mass absorption coefficients at 23.8 and 31.4 GHz. For these reasons (i.e., the inability to fit the AERI spectra as well as the inconsistent results that arise at the lower frequencies), we have elected to not use the more recent temperature-dependent infrared refractive indices in the MIXCRA retrievals in favor of the temperature-independent values in this work.

C. Brightness Temperature Comparison and Estimated Effect on LWP Retrievals

A comparison of measured and modeled brightness temperatures can help us determine the impact of various dielectric model formulations on LWP retrievals. If one assumes that

TABLE II
PATH-AVERAGED LIQUID MASS ABSORPTION COEFFICIENTS (Np cm^{-1}) FOR THE 5 FREQUENCIES ESTIMATED FROM THE OBSERVATIONS USED IN THIS STUDY. AVERAGE CLOUD TEMPERATURES ARE EXPRESSED IN DEGREES CELSIUS

Frequency (GHz)	$-25 < T_{avg} < -15$ (°C)	$-20 < T_{avg} < -10$ (°C)	$-15 < T_{avg} < -5$ (°C)	$-10 < T_{avg} < 0$ (°C)	$-5 < T_{avg} < 5$ (°C)
23.8	2.01± 0.42 N=235	1.62 ± 0.66 N=570	1.49± 0.53 N=971	1.47±0.44 N=753	1.32± 0.63 N=162
31.4	2.83±0.88 N=235	2.41±0.83 N=570	2.50±0.78 N=971	2.51±0.73 N=753	2.07±0.92 N=162
90.	6.43±1.81 N=34	5.17 ± 2.76 N=6	9.41± 4.03 N=140	10.47± 3.24 N=449	10.88± 2.50 N=465
150.	6.36±4.84 N=34	11.55±6.46 N=6	16.09± 5.28 N=140	18.70±3.84 N=465	18.95±3.84 N=465
170.	7.52 ± 3.69 N=188	11.54±4.75 N=563	13.48±3.89 N=380	-	-

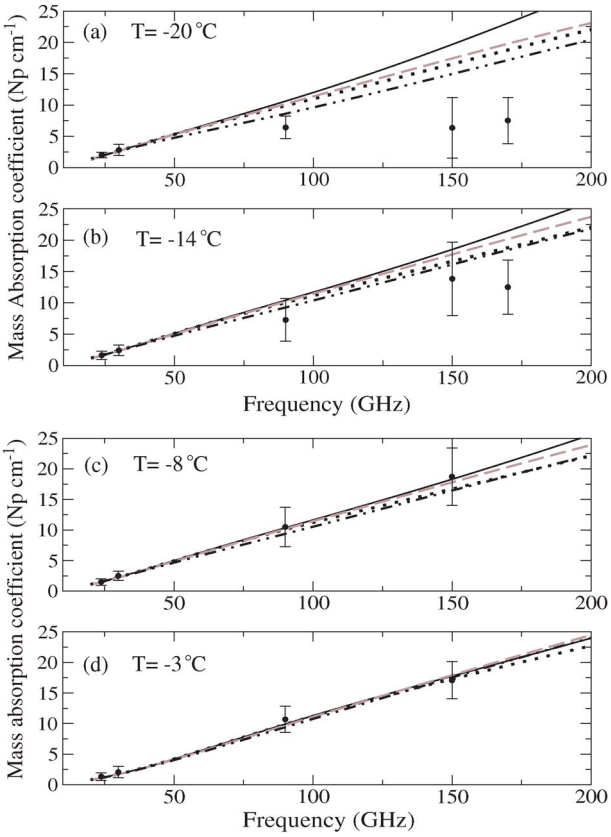

Fig. 5. Estimated and calculated mass absorption coefficients as a function of frequency (23.8, 31.4, 90.0, 150.0, and 170.0 GHz) and four representative temperatures: -20 °C, -14 °C, -8 °C, and -3 °C from top to bottom. Points with error bars (± 1 standard deviation) are estimated from brightness temperature measurements. Models are Liebe-91 (solid), Liebe-93 (dotted), Ellison-06 (dashed), and Stogryn-95 (dot-dashed).

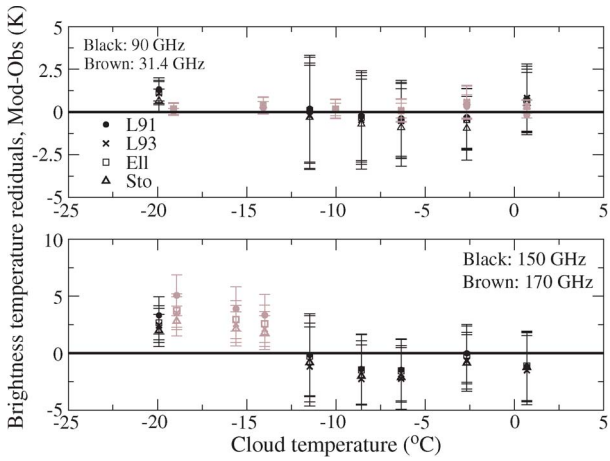

Fig. 6. Differences between simulated and observed brightness temperatures as a function of cloud mean temperature for clouds with LWP between 10 and 55 g/m^2. Top panel: 90 GHz (black), 31.4 GHz (brown). Bottom panel: 150 GHz (black), 170 GHz (brown).

the measured brightness temperatures are the "truth", then the magnitude of the residuals, in conjunction with an estimated sensitivity of each channel to liquid water, is indicative of the resulting error introduced in the retrievals by an error in the modeled brightness temperature. Brightness temperatures at 31.4, 90, 150, and 170 GHz were computed from radiosondes profiles with a uniformly distributed cloud layer inserted between the estimated cloud boundaries.

Brightness temperature residuals (model—measured) are shown in Fig. 6. In the top panel differences are shown for the 31.4 GHz (brown) and 90 GHz (black) channels. In the low LWP regime analyzed here, the four models have, as expected, similar residuals. The 31.4 GHz channel has the lowest sensitivity to LWP, especially when the LWP is low, and thus this channel will not be included in the following discussion. Measurements from the 90 GHz channel agree with models within error bars except for the coldest bin where all models slightly overestimate the brightness temperature. At this temperature the Stogryn-95 model has the lowest average residual (< 1 K). In the bottom panel the 150 GHz and 170 GHz residuals are shown. Here, the agreement between models and measurements is within error bars (1 standard deviation of the measurements) until temperatures become colder than approximately -15 °C, where all models produce brightness temperatures that are on average 2–5 K warmer than observations. At these higher frequencies the Stogryn-95 and Liebe-91 models produce the best and worst agreement with the measurements, respectively. When the temperature is between -10 °C and 0 °C all models have a slightly negative bias. This would indicate a slight underestimation of brightness temperatures by the models.

Although the LWP range examined here is limited, mid-level supercooled liquid clouds at these temperatures generally contain very small amounts of liquid water; clouds in

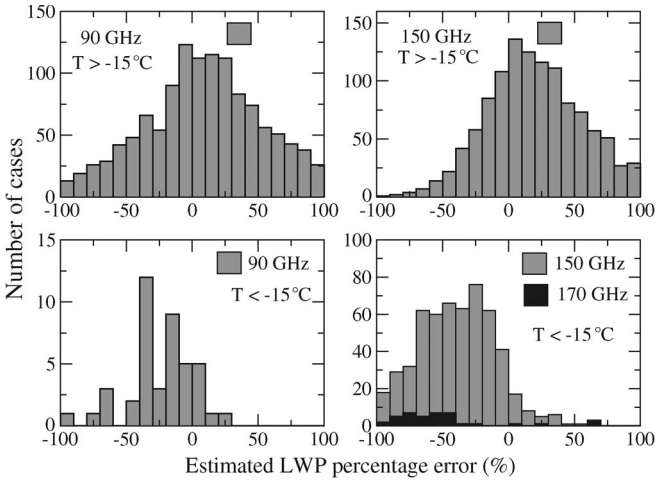

Fig. 7. Left column: Distribution of estimated LWP percentage error obtained with the 90 GHz frequency observations and the Stogryn-95 model for cases of cloud average temperature above (top) and below (bottom) -15 °C. Right column: same as in the left column, but for the 150 and 170 GHz frequencies.

orographic terrain can frequently have larger amounts of supercooled liquid water (e.g., [35]). Therefore, the magnitude of the residuals encountered here is likely representative of what can be expected in many mid-troposphere cloud situations when the cloud temperature is below -10 °C. It is possible that part of the noise in the MWRHF residuals for cases with $T_{\rm avg} > -15$ °C (where the single-phase AERI retrieval was enabled) could be due to undetected ice, which would result in a bias in the AERI-retrieved LWP. This is probably the case for some of the points that display high standard deviations around $T_{\rm avg} \sim -12$°C.

From the magnitude of the residuals shown in Fig. 6, one can, based on the sensitivity of the MWRHF and GVRP channels to LWP variations, estimate the resulting effect on the retrieved LWP when the retrieval is in a linear range. Expressing the results as a percentage error provides information that can be extrapolated to thicker clouds up to at least 100 g/m^2. Fig. 7 shows the distributions of expected LWP percentage errors for two temperature ranges (warmer and colder than -15 °C), where different liquid-sensitive frequencies were used in the retrieval. The histograms shown in Fig. 7 were produced by using the Stogryn-95 model, which agrees more closely with the observations as indicated in Figs. 4–6; thus, the LWP percentage errors is larger for the other three absorption models (especially if one uses the 150 and 170 GHz channels). Measured brightness temperatures were assumed to be the "truth" and the channel sensitivity to LWP was estimated as $\Delta{\rm LWP} = c\Delta T_b$ with $c \sim 4.83$ K^{-1}gm^{-2} at 90 GHz and $c \sim 3.91$ K^{-1}gm^{-2} at 150 and 170 GHz. The distribution of the LWP errors is shown for the 90 GHz channel in the two left panels (top and bottom). In the upper panel (warmer temperatures) the LWP does not show any appreciable bias. In the bottom panel the LWP is underestimated 25% on average. The corresponding distributions for the 150 and 170 GHz channels are shown in the right panels. At warmer temperatures (top panel—150 GHz) the LWP distribution does not show any appreciable bias; however, in colder clouds (bottom panel, 150 and 170 GHz) the Stogryn-95 model underestimates LWP by roughly 50%. If the same computations are repeated with the Liebe-91 model, the resulting underestimation at low temperatures is $\sim$50% at 90 GHz and $\sim$80% at 150 and 170 GHz. The high standard deviation of the histograms is a consequence of the fact that brightness temperature computations are affected by the compounding uncertainties previously discussed.

These results, in conjunction with the previous discussion on the residuals suggest that the Stogryn-95 model (followed by the Ellison model) would produce a more realistic LWP estimate than the Liebe-91 model if frequencies higher than 90 GHz were used in the retrievals. If the 90 GHz channel is used, all models will provide good estimate of LWP, with the Stogryn-95 model possibly producing slightly higher values than the other models at very cold temperatures. Although the residuals shown are admittedly small and experimental uncertainties may be affecting the results, the consistent behavior between the two instruments (located in different locations, built and calibrated differently) lends support to the validity of the conclusion. Additional support may come from the GVR, where LWP retrievals routinely obtained at the NSA from this instrument (which employs two double-sideband frequencies at 183.31 $\pm$ 7 and $\pm$ 14 GHz) with the Liebe-93 model are generally smaller than corresponding retrievals from the MWR as reported in [26].

V. Conclusion

This study was motivated by the need to assess how models of water complex permittivity affect the retrieval of cloud liquid water at microwave frequencies between 90 and 170 GHz in supercooled liquid clouds. For this purpose a data set was assembled of measurements from four ground-based DOE-ARM microwave radiometers in two locations. The data set provided sky brightness temperature measurements at 23.8, 31.4, 90, 150, and 170 GHz. An ancillary data set of measurements from a cloud radar, Vaisala ceilometer, Vaisala RS92 radiosondes, and AERI was used to derive additional information (such as cloud boundaries, cloud temperature, and cloud LWP) that could be used as input to a radiative transfer code. The cloud temperatures in the assembled data set ranged from 0 °C to approximately -22 °C. From the measurements it was possible to estimate a path-averaged mass absorption coefficient that could be compared with model computations. In spite of the limitations due to the experimental setup, the comparison between the observations and the model computations provided an interesting glimpse into possible issues affecting the extrapolation of available laboratory data of ε to cold temperatures and high frequencies.

The model computations were repeated with four formulations of the dielectic constant of water. From the comparison all models appear to perform reasonably well in a wide range of temperatures between 0 °C and -15 °C. Larger differences between the models appear at the two higher frequencies (150 and 170 GHz) when the cloud temperature is colder than -15 °C. In this case the measurements appear to be in better agreement with the Stogryn-95 model. In this temperature region, the Liebe-91 model displays the largest disagreement with the measurements. Previous studies such as those of [4], [12] reported conflicting results on the Stogryn-95 formulation.

A more recent study by Mätzler [37], however found that in supercooled clouds the Stogryn-95 model had the best agreement with observations in the 20–30 GHz range. Measured and simulated brightness temperatures were compared in a similar fashion, and from the magnitude of the residuals an estimate of the LWP error was derived. From this exercise it appears that, in case of extremely cold clouds, the error introduced by the models at frequencies above 90 GHz can cause an underestimation of LWP as low as -50% (for Stogryn-95) and as high as -80% (for Liebe-91). If confirmed by further studies, the magnitude of these errors suggest that, until better fits are derived for the water permittivity at higher frequencies and at cold temperatures, the advantages provided by the higher sensitivity of these channels are offset by the increased inaccuracy in the liquid water absorption models.

In this scenario the use of the 90 GHz frequency for the retrieval of LWP in supercooled clouds appears a safer choice. The results suggest that the models are in acceptable agreement with observations at this frequency and even in extremely cold cases the LWP errors will not exceed $\sim 25\%$ (except if Liebe-91 is used, in which case they could be higher). This frequency is therefore a good candidate to reduce the current uncertainty in the LWP retrieval of thin clouds to approximately 15%–30% in most temperature regimes.

From our data set we cannot to speculate which component of the dielectric constant formulation is causing the observed behavior. Unfortunately from measurements of brightness temperatures it is not possible to separate the real and imaginary part of ε. For this purpose laboratory measurements are necessary and it is highly desirable that, if feasible, more laboratory measurements be conducted in the high-frequency and low-temperature region (right now the only laboratory data available at low temperatures are those of [38] collected at 9.61 GHz). On the observational side additional radiometric data are soon going to be available. The GVRP is now continuously operating at the NSA site, and a 90 GHz radiometer will soon be deployed permanently at the same site. It is the intention of the authors to pursue this line of study by adding models to future comparison.

ACKNOWLEDGMENT

The data used in this study were collected as part of the U.S. Department of Energy (DOE) Atmospheric Radiation Measurement (ARM) program, which is sponsored by the Office of Science, Office of Biological and Environmental Research, Climate and Environmental Sciences Division.

REFERENCES

[1] E. H. Grant, T. J. Buchanan, and H. F. Cook, "Dielectric behavior of water at microwave frequencies," *J. Chem. Phys.*, vol. 26, no. 1, pp. 156–161, Jan. 1957.

[2] P. S. Ray, "Broadband complex refractive indices of ice and water," *Appl. Opt.*, vol. 11, no. 8, pp. 1836–1844, Aug. 1972.

[3] H. J. Liebe, G. A. Hufford, and T. Manabe, "A model for the complex permittivity of water at the frequencies below 1 THz," *Int. J. Infrared Millim. Waves*, vol. 12, no. 7, pp. 659–675, Jul. 1991.

[4] T. Meissner and F. J. Wentz, "The complex dielectric constant of pure and sea water from microwave satellite observations," *IEEE Trans. Geosci. Remote Sens.*, vol. 42, no. 9, pp. 1836–1849, Sep. 2004.

[5] D. D. Turner, A. M. Vogelmann, R. T. Austin, J. C. Barnard, K. Cady-Pereira, J. C. Chiu, S. A. Clough, C. Flynn, M. M. Khaiyer, J. Liljegren, K. Johnson, B. Lin, C. Long, A. Marshak, S. Y. Matrosov, S. A. McFarlane, M. Miller, Q. Min, P. Minnis, W. O'Hirok, Z. Wang, and W. Wiscombe, "Thin liquid water clouds: Their importance and our challenge," *Bull. Amer. Meteorol. Soc.*, vol. 88, no. 2, pp. 177–190, Feb. 2007.

[6] J. C. Liljegren, E. E. Clothiaux, G. G. Mace, S. Kato, and X. Dong, "A new retrieval for cloud liquid water path using a ground-based microwave radiometer and measurements of cloud temperature," *J. Geophys. Res.*, vol. 106, no. D13, pp. 14 485–14 500, 2001.

[7] D. D. Turner, S. A. Clough, J. C. Liljegren, E. E. Clothiaux, K. E. Cady-Pereira, and K. L. Gaustad, "Retrieving liquid water path and precipitable water vapor from the atmospheric radiation measurement (ARM) microwave radiometers," *IEEE Trans. Geosci. Remote Sens.*, vol. 45, no. 11, pp. 3680–3690, Nov. 2007.

[8] S. Crewell and U. Löhnert, "Accuracy of cloud liquid water path from ground-based microwave radiometry 2. Sensor accuracy and synergy," *Radio Sci.*, vol. 38, no. 3, p. 8042, 2003, DOI: 10.1029/202RS002634.

[9] E. R. Westwater, Y. Han, M. D. Shupe, and S. Y. Matrosov, "Analysis of integrated cloud liquid and precipitable water vapor retrievals from microwave radiometers during the Surface Heat Budget of the Arctic Ocean project," *J. Geophys. Res.*, vol. 106, no. D23, pp. 32 019–32 030, 2001.

[10] P. Zuidema, E. R. Westwater, C. Fairall, and D. Hazen, "Ship-based liquid water path estimates in marine stratocumulus," *J. Geophys. Res.*, vol. 110, p. D20 206, 2005, DOI: 10.1029/2005JD005833.

[11] A. E. Lipton, M. K. Griffin, and A. G. Ling, "Microwave transfer model differences in remote sensing of cloud liquid water at low temperatures," *IEEE Trans. Geosci. Remote Sens.*, vol. 37, no. 1, pp. 620–623, Jan. 1999.

[12] J. R. Wang, "A comparison of the MIR-estimated and model-calculated fresh water surface emissivity at 89, 150 and 220 GHz," *IEEE Trans. Geosci. Remote Sens.*, vol. 40, no. 6, pp. 1356–1365, Jun. 2002.

[13] W. J. Ellison, "Permittivity of pure water at standard atmospheric pressure, over the frequency range 0–25 THz and the temperature range 0 °C–100 °C," *J. Phys. Chem. Ref. Data*, vol. 36, no. 1, pp. 1–18, Mar. 2007.

[14] T. J. Hewison, D. Cimini, L. Martin, C. Gaffard, and J. Nash, "Validating clear air absorption models using ground-based microwave radiometers and vice versa," *Meteorol. Zeitschrift*, vol. 15, no. 1, pp. 27–36, Feb. 2006.

[15] J. C. Liljegren, S.-A. Boukabara, K. Cady-Pereira, and S. A. Clough, "The effect of the half-width of the 22-GHz water vapor line on retrievals of temperature and water vapor profiles with a 12-channel microwave radiometer," *IEEE Trans. Geosci. Remote Sens.*, vol. 43, no. 5, pp. 1102–1108, May 2005.

[16] D. D. Turner, M. P. Cadeddu, U. Lohnert, S. Crewell, and A. M. Vogelmann, "Modifications to the water vapor continuum in the microwave suggested by ground-based 150-GHz observations," *IEEE Trans. Geosci. Remote Sens.*, vol. 47, no. 10, pp. 3326–3337, Oct. 2009.

[17] M. P. Cadeddu, V. H. Payne, S. A. Clough, K. Cady-Pereira, and J. C. Liljegren, "The effect of the oxygen line-parameter modeling on temperature and humidity retrievals from ground-based microwave radiometers," *IEEE Trans. Geosci. Remote Sens.*, vol. 45, no. 7, pp. 2216–2223, Jul. 2007.

[18] H. J. Liebe, G. A. Hufford, and M. G. Cotton, "Propagation modeling of moist air and suspended water/ice particles at frequencies below 1000 GHz," in *Proc. AGARD*, 1993, vol. 542, pp. 1–10.

[19] A. P. Stogryn, H. T. Bull, K. Rubayi, and S. Iravanchy, "The microwave permittivity of sea and fresh water," GenCorp Aerojet, Azusa, CA, 1995, Aerojet Rep.

[20] W. Ellison, "Dielectric properties of natural media," in *Thermal Microwave Radiation: Application for Remote Sensing*. London, U.K.: IET Publisher, 2006, ser. The institution of Engineering and Technology (IET) Electromagnetic Waves series 52.

[21] T. P. Ackerman and G. M. Stokes, "The atmospheric radiation measurement program," *Phys. Today*, vol. 56, no. 1, pp. 38–44, 2003.

[22] D. Cimini, F. Nasir, E. R. Westwater, V. H. Payne, D. D. Turner, E. J. Mlawer, M. L. Exner, and M. Cadeddu, "Comparison of ground-based millimeter-wave observations and simulations in the Arctic winter," *IEEE Trans. Geosci. Remote Sens.*, vol. 47, no. 9, pp. 3098–3106, Sep. 2009, DOI: 10.1109/TGRS.2009.2020743.

[23] J. C. Liljegren, "Automatic self-calibration of ARM microwave radiometers," in *Microwave Radiometry and Remote Sensing of the Earth's Surface and Atmosphere*, P. Pampaloni and S. Paloscia, Eds. Lorton, VA: VSP Book, 2000, pp. 433–443.

[24] K. E. Cady-Pereira, M. W. Shephard, D. D. Turner, M. J. Mlawer, S. A. Clough, and T. J. Wagner, "Improved daytime column-integrated precipitable water vapor from Vaisala radiosondes humidity sensors,"

J. Atmos. Ocean. Technol., vol. 25, no. 6, pp. 873–883, Jun. 2008, DOI: 10.1175/2007JTECHA1027.1.

[25] M. P. Cadeddu, J. C. Liljegren, and A. L. Pazmany, "Measurements and retrievals from a new 183-GHz water-vapor radiometer in the arctic," *IEEE Trans. Geosci. Remote Sens.*, vol. 45, no. 7, pp. 2207–2215, Jul. 2007.

[26] M. P. Cadeddu, D. D. Turner, and J. C. Liljegren, "A neural network for real-time retrievals of PWV and LWP from arctic millimeter-wave ground-based observations," *IEEE Trans. Geosci. Remote Sens.*, vol. 47, no. 7, pp. 1887–1900, Jul. 2009.

[27] V. H. Payne, J. S. Delamere, K. E. Cady-Pereira, R. R. Gamache, J.-L. Moncet, E. J. Mlawer, and S. A. Clough, "Air-broadened half-widths of the 22- and 183-GHz water-vapor lines," *IEEE Trans. Geosci. Remote Sens.*, vol. 46, no. 11, pp. 3601–3617, Nov. 2008, DOI: 10.1109/TGRS.2008.2002435.

[28] D. D. Turner, "Arctic mixed-phase cloud properties from AERI lidar observations: Algorithm and results from SHEBA," *J. Appl. Meteorol.*, vol. 44, no. 4, pp. 427–444, Apr. 2005.

[29] D. D. Turner, "Improved ground-based liquid water path retrievals using a combined infrared and microwave approach," *J. Geophys. Res.*, vol. 112, p. D15 204, 2007, DOI: 10.1029/2007JD008530.

[30] R. O. Knuteson, H. E. Revercomb, F. A. Best, N. C. Ciganovich, R. G. Dedecker, T. P. Dirkx, S. C. Ellington, W. F. Feltz, R. K. Garcia, H. B. Howell, W. L. Smith, J. F. Short, and D. C. Tobin, "Atmospheric emitted radiance interferometer. Part II: Instrument performance," *J. Atmos. Oceanic Technol.*, vol. 21, no. 12, pp. 1777–1789, Dec. 2004.

[31] S. Crewell, K. Ebell, U. Löhnert, and D. D. Turner, "Can liquid water profiles be retrieved from passive microwave zenith observations?" *Geophys. Res. Lett.*, vol. 36, pp. L06 803, 2009, DOI: 10.1029/2008GL036934.

[32] F. T. Ulaby, R. K. Moore, and A. K. Fung, *Microwave Remote Sensing: Active and Passive, From Theory to Applications*, vol. 3. Dedham, MA: Artech House, 1986.

[33] H. D. Downing and D. Williams, "Optical constants of water in the infrared," *J. Opt. Soc. Amer.*, vol. 61, pp. 1107–1110, 1974.

[34] A. Y. Zasetsky, A. F. Khalizov, M. E. Earle, and J. J. Sloan, "Frequency dependent complex refractive indices of supercooled liquid water and ice determined from extinction spectra," *J. Phys. Chem. A*, vol. 109, no. 12, pp. 2760–2764, Mar. 2005.

[35] R. Wagner, S. Benz, O. Möhler, H. Saathoff, M. Schnaiter, and U. Schurath, "Mid-infrared extinction spectra and optical constants of supercooled water droplets," *J. Phys. Chem. A*, vol. 109, no. 32, pp. 7099–7112, Aug. 2005.

[36] U. Löhnert, S. Kneifel, A. Battaglia, M. Hagen, L. Hirsch, and S. Crewell, "A multi-sensor approach toward a better understanding of snowfall microphysics: The TOCSA project," *Bull. Amer. Meteorol. Soc.*, 2011, DOI: 10.1175/2010BAMS2909.1.

[37] C. Mätzler, P. W. Rosenkranz, and J. Cermak, "Microwave absorption of supercooled clouds and implications for the dielectric of water," *J. Geophys. Res.*, vol. 115, p. D23 208, 2010, DOI: 10.1029/2010JD014283.

[38] D. Bertolini, M. Cassettari, and G. Salvetti, "The dielectric relaxation time of supercooled water," *J. Chem. Phys.*, vol. 76, no. 6, pp. 3285–3290, Mar. 1982.

Maria P. Cadeddu received the Laurea degree in physics from the University of Cagliari, Cagliari, Italy, in 1994 and the Ph.D. degree in physics from Heriot-Watt University, Edinburgh, U.K., in 2002.

Since 2005, she has been with the Argonne National Laboratory where her primary duty has been as the Instrument Mentor for the U.S. Department of Energy Atmospheric Radiation Measurement Program microwave radiometer instrumentation. Her research interests include microwave radiometers, application of remote sensing to atmospheric research, and inversion theory.

Dr. Cadeddu is a member of the American Geophysical Union.

David D. Turner received the B.A. and M.S. degrees in mathematics from Eastern Washington University, Cheney, WA, in 1992 and 1994, respectively, and the Ph.D. degree in atmospheric science from the University of Wisconsin—Madison, Madison, in 2003.

He is currently a Physical Scientist at the NOAA National Severe Storms Laboratory in Norman, Oklahoma. He is actively involved in the Department of Energy's Atmospheric Radiation Measurement (ARM), Argonne, IL, and Atmospheric System Research (ASR), Washington, DC, programs, serving as a Co-Chair of the ASR Cloud-Aerosol-Precipitation Interactions working group, the Chair of the ARM Climate Research Facility Science Board, and a Member of the ASR Science and Infrastructure Steering Committee. His current research interests include infrared and microwave remote sensing and radiative transfer in clear and cloudy atmospheres; retrieval theory and information content; boundary layer evolution over the diurnal cycle; and measuring water vapor, cloud, and aerosol properties from active and passive remote sensors.

Dr. Turner is a member of the American Meteorological Society and the American Geophysical Union.